MODELING THE PIEZORESISTIVE BEHAVIOR OF CARBON FIBER REINFORCED CEMENT

Sirong Zhu, Sihai Wen, and D.D.L. Chung†, University at Buffalo, State University of New York, Buffalo, NY 14260-4400*

*Permanent address: Department of Engineering Structures and Mechanics, School of Science, Wuhan University of Technology, Wuhan, Hubei, China 430070.
†Corresponding author: ddlchung@buffalo.edu, Fax. (716) 645-3875; Tel. (716) 645-2593 X2243. **http://alum.mit.edu/www/ddlchung**.

Abstract

Piezoresistivity (change of the electrical resistivity with strain) allows cement reinforced with short carbon fiber to sense strain/stress. The fiber volume fraction can be below the percolation threshold. The volume resistivity increases reversibly upon uniaxial tension and decreases reversibly upon uniaxial compression. Upon flexure, the surface resistance on the tension side increases reversibly, while that on the compression side decreases reversibly. The phenomenon, which is modeled analytically in this work, is considered to be due to the slight pull-out of crack-bridging fibers during crack opening and the consequent increase in the contact electrical resistivity of the fiber-matrix interface. Good agreement is found between calculated and experimental results.

Introduction

Cement reinforced with short carbon fibers has been shown to be able to sense its own strain (Chung, 2002; Wen and Chung, 2000, 2001, 2005, 2006a, 2006b, 2006c, 2007) and damage (Wen and Chung, 2006a, 2006b, 2006c) by DC electrical resistance measurement. The ability of a structural material to sense itself is known as self-sensing. Compared to the conventional method of attaining sensing by the use of embedded or attached sensors, self-sensing is advantageous in its low cost, high durability, large sensing volume and absence of mechanical property loss. In contrast, the use of embedded sensors tends to cause mechanical property loss to the structure.

The attributes in self-sensing can be strain (which relates to the stress), damage, temperature, etc. This paper is focused on the sensing of strain. Strain sensing is valuable for structural vibration control, weighing, traffic monitoring, border security, building facility management and other applications.

The self-sensing of strain can be attained by using piezoresistivity, i.e., the reversible effect of strain on the electrical resistance. The effectiveness of this method of self-sensing has been shown by experimental results obtained on carbon fiber reinforced cement during tension, compression and flexure (Wen and Chung, 2005, 2006a, 2006b, 2006c, 2007a). Upon uniaxial compression, the volume resistance decreases (due to the slight push-in of crack-bridging fibers and the consequent decrease of the contact electrical resistivity of the fiber-cement interface); upon uniaxial tension, the volume resistance increases (due to the slight pull-out of crack-bridging fibers and the consequent decrease of the contact resistivity); upon flexure, the surface resistance on the tension side increases (as in the case of uniaxial tension), while that on the compression side decreases (as in the case of uniaxial compression).

In the case of flexural loading, it has been shown that the piezoresistivity is enhanced by the presence of embedded steel reinforcing bars (rebars) (Wen and Chung, 2006a). Steel rebars are commonly used for reinforcing concrete, so the effect of the presence of steel rebars on the piezoresistivity is relevant to practical implementation of the self-sensing.

Theoretical work is important for fundamental understanding of the piezoresistive phenomenon. In addition, a model of the phenomenon facilitates practical implementation, as it allows the prediction of the extent of resistance change for a given amount of deformation in a structure of arbitrary dimensions. This paper describes the modeling of the phenomenon, based on a mechanism involving slight fiber pull-out upon crack opening (push-in upon crack closing) and the consequent increase (decrease) in the contact electrical resistivity of the fiber-matrix interface. This model has been applied to the cases of uniaxial tension and uniaxial compression, without steel reinforcing bars, in addition to the case of flexural loading, both with and without embedded steel reinforcing bars.

Basic theory of piezoresistivity in carbon fiber cement

The basic theory of piezoresistivity in carbon fiber cement is described in this section in terms of the effect of uniaxial loading on the volume resistance. Consider a cement element containing a carbon fiber under stress σ_x in the x direction. The angle between the fiber and σ_x is α. Let the crack length perpendicular to the fiber be a. Crack opening and closing occur only in the presence of tensile and compressive stresses respectively in the direction perpendicular to the plane of the crack. This normal stress σ_α, which is in the direction of the fiber, can be expressed as

$$\sigma_\alpha = \frac{\sigma_x}{2} + \frac{\sigma_x}{2}\cos 2\alpha \qquad (1)$$

This normal stress gives rise to a force F_f acting in the direction of the fiber. This force is the pull-out force on the fiber. It is given by

$$F_f = at\sigma_\alpha = \tau A_c = \tau \cdot \pi d h_f, \qquad (2)$$

where t is the thickness of the crack, τ is shear stress between the fiber and cement, A_c is contact area between the fiber and cement, d is the diameter of the fiber, and h_f is the length of the contact (interface) between the fiber and cement.

According to the equations of equilibrium,

$$\tau = \frac{at\sigma_\alpha}{\pi d h_f} \qquad (3)$$

The electrical resistance of the specimen under study is contributed by conduction paths within the cement matrix surrounding a crack with the bridging fiber, in addition to the bridging fiber itself. The change in electrical resistance ΔR_s during loading is mainly contributed by the change in the contact resistance ΔR_c of the interface between fiber and cement, i.e.,

$$\Delta R_s = \Delta R_c \qquad (4)$$

Single fiber pull-out testing [22] showed that the contact resistivity of the interface between carbon fiber and cement gradually increases with increasing shear stress prior to the abrupt increase when the shear stress reaches its maximum. For simplicity, we assume that the contact resistance increases linearly with the shear stress τ. Thus,

$$\Delta R_s = c\tau = c\frac{at}{\pi d h_f}\left(\frac{\sigma_x}{2} + \frac{\sigma_x}{2}\cos 2\alpha\right) \qquad (5)$$

where c is a proportionality constant. Eq. (5) shows that the change in resistance due to piezoresistivity depends on the fiber direction. Different fiber directions result in different levels of strain sensitivity.

Based on the data shown in Fig. 2 of Fu and Chung (1995), the curve of contact resistivity versus shear stress can be obtained. The slope k of this curve is

$$k = 0.1764 \times 10^5\ \Omega.cm^2/MPa = 1.764 \times 10^{-6}\ \Omega.m^2/Pa \qquad (6)$$

Since $\Delta R_s = \Delta R_c = \Delta(\rho_c/A_c) = \Delta(\rho_c/\pi d\, h_f) = c\tau$,

$$c = k/A_c = k/\pi d\, h_f = 1.764 \times 10^{-6}/\pi d\, h_f\ (\Omega.m^2/Pa) \qquad (7)$$

Using Eq. (3) and (7),

$$\Delta R_s = \frac{1.764\times10^{-6} at}{2\left(\pi d h_f\right)^2}\sigma_x(1+\cos 2\alpha) \tag{8}$$

The carbon fibers in cement are distributed randomly. Although there is a slight tendency for the fibers to lie down in the horizontal plane during setting and curing, the degree of preferred orientation is slight and is negligible when the specimen is more than 25 mm high in the vertical direction during setting and curing (Wen and Chung, 2005). A high degree of fiber dispersion is attained by the use of silica fume and methylcellulose as admixtures and by ozone treatment of the fiber prior to using the fiber; these fiber dispersion techniques were indeed used in the experimental work (Wen and Chung, 2006a) that provided the experimental results employed in this paper for comparison between theoretical and experimental results. Thus, it can be considered that, on the average, every fiber has the same contribution to the piezoresistive effect. Therefore, ΔR_s can be averaged from $\alpha = 0°$ to 90°, thereby removing the dependence on α. Integrating both sides of Eq. (5) with respect to α and taking the average value over α, we have

$$\begin{aligned}\Delta R_s &= \frac{2}{\pi}\int_0^{\frac{\pi}{2}} c\frac{at}{\pi d h_f}\left(\frac{\sigma_x}{2}+\frac{\sigma_x}{2}\cos 2\alpha\right)d\alpha \\ &= \frac{cat}{2\pi d h_f}\sigma_x \\ &= \frac{1.764\times10^{-6} at}{2\pi^2 d^2 {h_f}^2}\sigma_x\end{aligned} \tag{9}$$

Distribution of carbon fibers in cement

Different fiber volume fractions result in different numbers of fibers in a carbon fiber cement element. Let the fiber volume fraction be C_f, the volume of a carbon fiber cement specimen be V, and the length of a carbon fiber be l_f. Then the volume of all the fibers in the specimen is

$$V_f = C_f V \tag{10}$$

and the number of fibers is

$$N = \frac{V_f}{\frac{\pi}{4}d^2 l_f} \tag{11}$$

Under the condition of uniform fiber distribution, it can be considered that the ends of all fibers (one end of every fiber being considered as the position of the fiber) are uniformly distributed, with every fiber end occupying a small cube of volume V_o:

$$V_o = \frac{V}{N} = \frac{\frac{\pi}{4}d^2 l_f}{C_f} \tag{12}$$

The distance S between the ends of two adjacent fibers is the length of an edge of the small cube, that is

$$S = \sqrt[3]{V_o} = \sqrt[3]{\frac{\frac{\pi}{4}d^2 l_f}{C_f}} \tag{13}$$

In the experiment, d = 15 μm and l_f = 5 mm. When C_f = 0.48%, S = 0.57 mm.

Modeling the electrical resistance

Modeling the surface electrical resistance

The surface electrical resistance is the resistance measured by using electrical contacts that are on one surface of a specimen, as illustrated in Fig. 1, where the contacts are on the tension surface (for measuring the tension surface resistance) and on the compression surface (for measuring the compression surface resistance) of a specimen under flexure. The surface current contacts allow the current to be injected from one surface, rather than being injected uniformly throughout the cross section of the

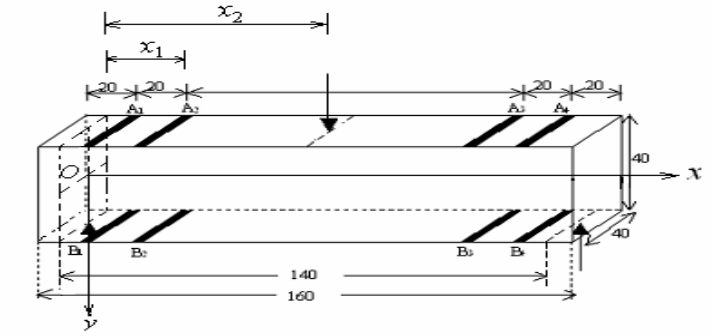

Fig. 1 Specimen configuration for flexural testing by three-point bending. The three points are shown by arrows. A_1, A_2, A_3 and A_4 are electrical contacts on the compression surface, whereas B_1, B_2, B_3 and B_4 are electrical contacts on the tension surface. All dimensions are in mm.

specimen. The surface voltage contacts allow the voltage to be measured on the surface. Thus, the surface resistance, as obtained by dividing the voltage between the surface voltage contacts by the current injected by the surface current contacts, is to be distinguished by the volume resistance, which is ideally measured by using current contacts that allow uniform current injection throughout the cross section. Due to the assumed uniformity of the current density in the cross section of the specimen in the case of volume resistance measurement, the volume resistance is simply related to the volume electrical resistivity of the specimen. However, due to the non-uniformity in the current density in the case of surface resistance measurement, the surface resistance is not simply related to the volume resistivity.

The use of the piezoresistivity under flexure mainly involves measurement of the surface resistance. This section provides a model for the surface resistance. The surface electrical resistance is measured using the surface electrical contacts shown in Fig. 1, where a carbon fiber cement beam is under flexure (three-point bending). The compression surface resistance was measured by using A_1 and A_4 as current contacts and A_2 and A_3 as voltage contacts. The tension surface resistance was measured by using B_1 and B_4 as current contacts and B_2 and B_3 as voltage contacts. The through-thickness resistance was measured by using A_1 and B_1 as current contacts and A_2 and B_2 as voltage contacts.

Because the stress is different at different points along the thickness of the beam, the resistance change varies. Hence, the beam is divided into n layers which are stacked in the thickness direction, such that each layer is of thickness equal to the distance S between the ends of adjacent fibers (Eq. (13)). Hence,

$$n = \frac{h}{S} \qquad (14)$$

In order to calculate the total change in resistance ΔR, we use an equivalent electrical circuit to describe the beam, as shown in Fig. 2. In each layer there are two resistances ($R_L(i)$ and $R_T(i)$) which correspond to two directions of electrical conduction, namely the longitudinal direction (x-axis) and the through-thickness direction (y-axis). Both resistances contribute to the surface resistance (whether at the tension or compression surface), which is the quantity measured.

In the equivalent circuit of Fig. 2, $R_L(i)$ is the longitudinal resistance of the ith layer. It is associated with an element of length L_V (the distance between the two inner contacts, A_2 and A_3, shown in Fig. 1), thickness S and width b. Hence,

$$R_L(i) = \frac{\rho L_V}{bS} \qquad (15)$$

where ρ is the volume electrical resistivity.

In the circuit of Fig. 2, $R_T(i)$ is the through-thickness resistance of the ith layer. The element associated with $R_T(i)$ is taken to be of length S in the through-thickness direction and width S in the longitudinal direction, since the current path actually bows into the specimen from the surface and the thickness of the bowed path is considered to be S. Hence,

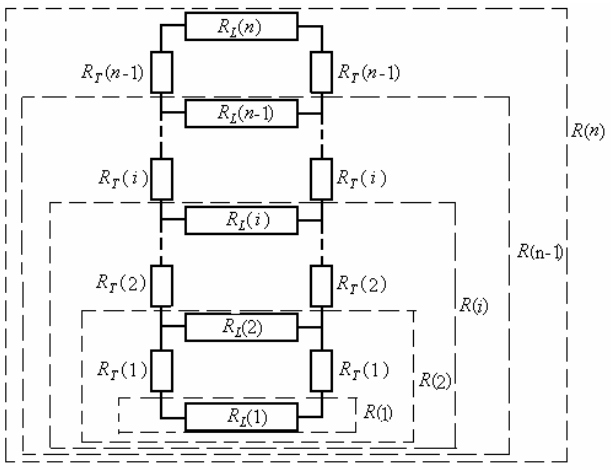

Fig. 2 Equivalent electrical circuit used for calculating the surface resistance.

$$R_T(i) = \frac{\rho S}{bS} \qquad (16)$$

In order to avoid counting the same element as contributing to both $R_L(i)$ and $R_T(i)$., L_V in Eq. (15) should be reduced by 2S. However, since 2S is small compared to L_V, this reduction is not performed in this work.

The top surface resistance $R(n)$, i.e., the resistance measured between the two terminals of resistor $R_L(n)$, is calculated by considering this surface resistance to be $R_L(n)$ in parallel with the sum of $R_T(n\text{-}1)$, $R_L(n\text{-}1)$ and $R_T(n\text{-}1)$ (these three resistances in series in Fig. 2). The resistance $R(i)$ between the two terminals of $R_L(i)$ is obtained by considering $R_L(i)$ in parallel with the sum of $R_T(i\text{-}1)$, $R_L(i\text{-}1)$ and $R_T(i\text{-}1)$.

$$R(1) = R_L(1) \qquad (17)$$

$$R(i) = \frac{(2R_T(i-1) + R(i-1))R_L(i)}{R_L(i) + 2R_T(i-1) + R(i-1)} \qquad (i = 1,.....,n) \qquad (18)$$

and

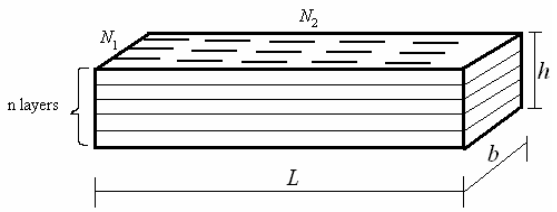

Fig. 3 Schematic illustration of the layers in the plane of the beam in the model for calculating the surface resistance. The fibers in the top layer are schematically illustrated by using short lines in the longitudinal direction.

$$R(n) = \frac{(2R_T(n-1) + R(n-1))R_L(n)}{R_L(n) + 2R_T(n-1) + R(n-1)} \qquad (19)$$

Although Eq. (19) gives the resistance measured between two points on the surface (i.e., A_2 and A_3 in Fig. 1), it can be used to calculate the resistance measured between the corresponding two points on any of the layers in Fig. 3.

Modeling the through-thickness resistance

The through-thickness resistance refers to the resistance measured between A_2 and B_2 in Fig. 1. This resistance is one of the measured quantities (Wen and Chung, 2006a), so this resistance is modeled.

The model of the surface resistance involves layers in the longitudinal direction for the purpose of calculating the longitudinal surface resistance $R(n)$ based on the values of R_T and R_L for the various layers. This model can be modified by having the layers perpendicular to the longitudinal direction for the purpose of calculating the through-thickness resistance, as illustrated in Fig. 4. In the modified model, the electrical circuit model of Fig. 2 is modified so that R_L is replaced by R_T and R_L is replaced by R_L. Hence, the through-thickness resistance is given by the following equation, which is obtained by modifying Eq. (19) as applied to the resistance between two points on an interior layer.

$$R(n) = \frac{(2R_L(n-1) + R(n-1))R_T(n)}{R_T(n) + 2R_L(n-1) + R(n-1)} \qquad (20)$$

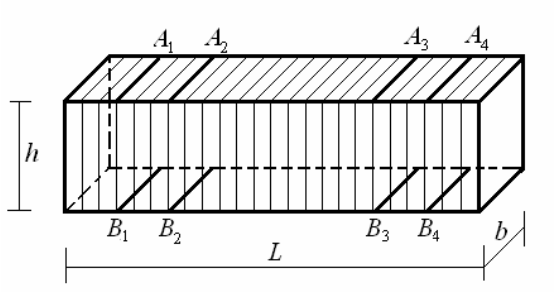

Fig. 4 Schematic illustration of the layers in the plane perpendicular to the longitudinal direction in the model for calculating the through-thickness resistance.

Comparison of measured and calculated resistance values

Calculation of the surface resistance was based on Eq. (19) and a value of the volume resistivity that was obtained either from the use of Eq. (19) and the measured surface resistance (Wen and Chung, 2006a) or from the use of Eq. (20) and the measured through-thickness resistance (Wen and Chung, 2006a). Calculation of the through-thickness resistance was based on Eq. (20) and a value of the volume resistivity that was obtained either from the use of Eq. (19) and the measured surface resistance (Wen and Chung, 2006a) or from the use of Eq. (20) and the measured through-thickness resistance (Wen and Chung, 2006a). Reasonably good agreement is found between the calculated and measured values for both the surface resistance and the through-thickness resistance.

Based on the measured surface resistance and the surface resistance model, the volume resistivity is found to be 1.84×10^5 Ω.cm. This value is high compared to the separately measured volume resistivity of 1.5×10^4 Ω.cm (Wen and Chung, 2005). This discrepancy is probably due to the presence of a surface layer which affects the surface resistance measurement. This layer may be different from the interior of the specimen in terms of the preferred orientation and concentration of the fibers, thus resulting in greater difficulty of current penetration. Such a surface layer is expected to affect strongly the measured surface resistance, though it has relatively little effect on the measured volume resistivity.

Piezoresistivity under flexure

Under flexure (three-point bending), the moment and normal stress are respectively

$$M = \frac{P}{2}x$$

$$\sigma_x = \frac{My}{I_z} = \frac{Pxy}{2I_z}, \tag{21}$$

where x is the position along the neutral axis of the beam, y is the distance from the neutral axis (Fig. 3), P is the force, and I_z is the moment of inertia of the cross section of the beam.

Combining Eq. (9) and (21) gives

$$\Delta R_s = \frac{catPxy}{4\pi d h_f I_z}$$

$$= \frac{1.764\times10^{-6}\, atPxy}{4\pi^2 d^2 {h_f}^2 I_z} \tag{22}$$

Eq. (22) shows the change of resistance of a cement specimen with a single carbon fiber under flexure. Actually, there are a large number of carbon fibers in a cement specimen and they are both in series and in parallel. Fig. 3 illustrates the fiber distribution, where all fibers are considered in the same direction (as justified by the angular averaging in Eq. (9) and the consequent removal of the angular dependence), such as the x direction in Fig. 1. There are N_1 fibers that are in parallel along the edge of length b, and there are N_2 fibers that are in series along the edge of length L, as shown in Fig. 3. From Eq. (22), the change of resistance depends on the location (i.e., the coordinates x and y) of the fiber.

Under flexure, the top part of the beam is compressed and both resistances in this part decrease, whereas the bottom part of the beam is tensioned and both resistances in this part increase. Although the longitudinal resistance is affected by flexure more than the through-thickness resistance, both resistances are affected in the same way. This notion is based on prior experimental results for carbon fiber cement under uniaxial compression (Wen and Chung, 2001) and uniaxial tension (Wen and Chung, 2000). Under uniaxial compression, both the longitudinal and transverse resistances increase; the transverse resistance increases in spite of the Poisson effect, which causes slight transverse shrinkage. Under uniaxial compression, both the longitudinal and transverse resistances decrease; the transverse resistance decreases in spite of the Poisson effect, which causes slight transverse elongation.

N_1 and N_2 are given by

$$N_1 = \frac{b}{S} \tag{23}$$

and

$$N_2 = \frac{N}{nN_1}. \tag{24}$$

Since the N_1 fibers in one row of fibers in a layer (Fig. 3) are electrically in parallel longitudinally (x-axis), they give a resistance change ΔR_1 that is equal to $1/N_1$ of that given by a single fiber. Hence,

$$\Delta R_1(i) = \frac{\Delta R_s}{N_1} = \frac{\dfrac{1.764\times10^{-6}\, atPxy_i}{4\pi^2 d^2 {h_f}^2 I_z}}{N_1} \tag{25}$$

Eq. (25) means that ΔR_1 is a function of x and y. Thus, it can be written as $\Delta R_1(x, y_i)$.

One layer consists of N_2 groups of N_1 fibers that are electrically in series along the x-axis. Hence, the resistance change due to the ith layer is

$$\Delta R_L(i) = \sum_{N_2} \Delta R_1(x, y_i) \tag{26}$$

In one layer, y is a constant. Hence, Eq. (26) shows that ΔR_1 is a linear function of x. By symmetry, the average value of $\Delta R_1(x, y)$ can be approximated as that at $x = \frac{x_1 + x_2}{2}$, where x_1 and x_2 are as defined in Fig. 3. Hence,

$$\begin{aligned} \Delta R_L(i) &= \sum_{N_2} \Delta R_1(x, y_i) = N_2 \frac{1.764\times10^{-6}\, atPxy_i}{4N_1 \pi^2 d^2 {h_f}^2 I_z} \\ &= \frac{1.764\times10^{-6} N_2}{8N_1 \pi^2 d^2 {h_f}^2 I_z} atPy_i (x_1 + x_2) \end{aligned} \tag{27}$$

Based on prior experimental results under uniaxial tension and uniaxial compression, the magnitude of the transverse gage factor (i.e., the fractional change in resistance in the transverse direction per unit strain in the transverse direction) is roughly the same as that of the longitudinal direction (Wen and Chung, 2000, 2001). Since the through-thickness strain is related to the longitudinal strain by the Poisson ratio ν,

$$\Delta R_T(i) = \nu \frac{R_T(i)}{R_L(i)} \Delta R_L(i) \tag{28}$$

In flexural experiments, the midspan deflection is a quantity that is usually measured. Therefore, ΔR in Eq. (27) and (28) needs to be expressed as a function of the midspan deflection f. For a beam under three-point bending,

$$f = \frac{PL^3}{48EI_z} \tag{29}$$

Combining Eq. (27), (28) and (29) gives

$$\Delta R_L(i) = \frac{1.764\times10^{-6}\times48EfN_2}{8N_1 \pi^2 d^2 {h_f}^2 L^3} aty_i (x_1 + x_2) \tag{30}$$

$$\Delta R_T(i) = \nu \frac{R_T(i)}{R_L(i)} \frac{1.764\times10^{-6}\times48EfN_2}{8N_1 \pi^2 d^2 {h_f}^2 L^3} aty_i (x_1 + x_2) \tag{31}$$

Eq. (30) and (31) give the change in the change in the resistance of the ith layer due to piezoresistivity. The parameter at in Eq. (30) and (31) describes the area of a crack.

Upon flexure, all the resistances in Fig. 3 change. Let $R_L(i)$, $R_T(i)$ and $R(i)$ change to $R'_L(i)$, $R'_T(i)$ and $R'(i)$ respectively. In other words,

$$R'_L(i) = R_L(i) + \Delta R_L(i) \quad (i = 1, ..., n) \tag{32}$$

$$R'_T(i) = R_T(i) + \Delta R_T(i) \quad (i = 1, ..., n-1) \tag{33}$$

$$R'(i) = \frac{(2R'_T(i-1) + R'(i-1))R'_L(i)}{R'_L(i) + 2R'_T(i-1) + R'(i-1)} \quad (i = 1, ..., n) \tag{34}$$

and

$$R'(n) = \frac{(2R'_T(n-1) + R'(n-1))R'_L(n)}{R'_L(n) + 2R'_T(n-1) + R'(n-1)} \tag{35}$$

Hence, the total change in the top surface resistance is given by

$$\Delta R = R'(n) - R(n) \tag{36}$$

and the fractional change of resistance is

$$\frac{\Delta R}{R(n)} = \frac{R'(n) - R(n)}{R(n)} \tag{37}$$

Comparison of measured and calculated piezoresistive behavior

(a)

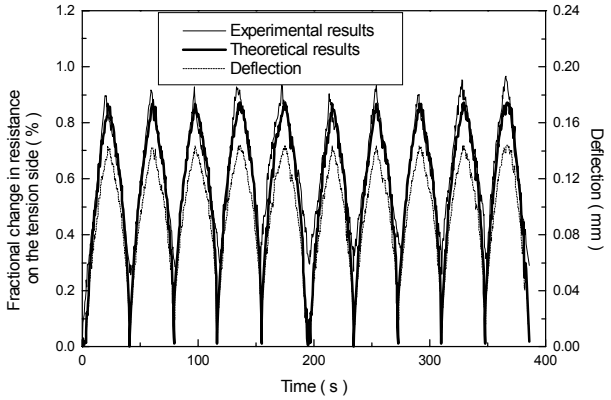

(b)

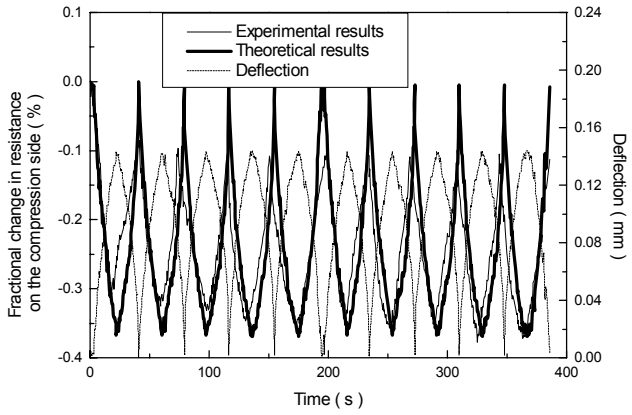

Fig. 5 Comparison of the calculated and measured curves for the change in surface resistance upon repeated flexure for carbon fiber cement beam without rebar. (a) The tension side. (b) The compression side. Measured results are from Wen and Chung (2006a).

The prior experimental work (Wen and Chung, 2006a), with the specimen beam as shown in Fig. 3, involves d = 15 μm, h_f = 5 mm (nominal fiber length is 5 mm), C_f = 0.48 vol.% (fibers in the amount of 0.5% by mass of cement), E =13 GPa (Wen and Chung, 2000, 2001), x_1 = 30 mm, and x_2 = 70 mm. Assume that $at = 1.9 \times 10^{-10}\, m^2$ for the tension side; $at = 8.5 \times 10^{-11}\, m^2$ for the compression side. It is reasonable that, at the same deflection, cracks are much larger at the tension side than the compression side.

The calculated and measured values of the change in surface resistance during repeated flexure at a maximum deflection f of 0.143 mm (experimental value of f in the first cycle) are compared in Fig. 5(a) and Fig. 5(b) for the tension and compression surfaces respectively. Comparison of the calculated and measured curves shows good agreement between them, although the partial irreversibility of the measured resistance change after the first cycle causes some difference after the first cycle. For the tension side, the measured

resistance is irreversibly increased after the first cycle; for the compression side, the measured resistance is irreversibly decreased after the first cycle. These irreversible effects are attributed to minor damage.

Under uniaxial tension, the volume resistance increases upon loading, such that there is slight partial irreversibility in the resistance increase after unloading (Wen and Chung, 2000). The irreversible increase is due to minor damage. This irreversible increase is consistent with the irreversible increase in the tension surface resistance during flexural loading (Wen and Chung, 2006a).

Under uniaxial compression, the volume resistance decreases upon loading, such that the resistance is irreversibly increased after unloading (Wen and Chung, 2001). This irreversible increase is not consistent with the irreversible decrease in the compression surface resistance during flexural loading (Wen and Chung, 2006a). This inconsistency for the compression case suggests that the type of damage under uniaxial compression is not the same as that at the compression surface during flexure. The stress is highest at the midspan position in case of flexure, thus causing the damage to be concentrated at the midspan position. On the other hand, the stress is uniformly distributed in case of uniaxial compression, so that the damage is spread out. Damage that is associated with an irreversible resistance decrease, as in the case of flexure, may be due to excessive crack closing, i.e., crack squeezing; this type of damage is relatively severe. Damage that is associated with an irreversible resistance increase, as in the case of uniaxial compression, may be due to an irreversible degradation of the fiber-matrix interface; this type of damage is relatively subtle.

Conclusion

A model for the piezoresistivity in carbon fiber reinforced cement is provided. This model explains the effect of flexure on the electrical resistance of the tension and compression surfaces of a beam. The model is based on the notion that the piezoresistivity is due to the slight pull-out of crack-bridging fibers during crack opening and the consequent increase in the contact electrical resistance of the fiber-matrix interface. Good agreement has been attained between calculated and measured results.

Acknowledgement

This work was supported in part by U.S. National Science Foundation and in part by the Key Project of National Natural Science Foundation of China under grant No. 50238040.

References

Chung, D. D. L. 2002. Piezoresistive cement-based materials for strain sensing. *J. Intelligent Material Systems and Structures* 13(9):599-609.

Fu, X. and Chung, D. D. L. 1995. Contact electrical resistivity between cement and carbon fiber: its decrease with increasing bond strength and its increase during fiber pull-out. *Cem. Concr. Res.* 25(7):1391-1396.

Wen, S. and Chung, D. D. L. 2000. Uniaxial tension in carbon fiber reinforced cement, sensed by electrical resistivity measurement in longitudinal and transverse directions. *Cem. Concr. Res.* 30(8):1289-1294.

Wen, S. and Chung, D. D. L. 2001. Uniaxial compression in carbon fiber reinforced cement, sensed by electrical resistivity measurement in longitudinal and transverse directions. *Cem. Conc. Res.* 31(2):297-301.

Wen, S. and Chung, D. D. L. 2005. Strain sensing characteristics of carbon fiber reinforced cement. *ACI Mater. J.* 102(4):244-248.

Wen, S. and Chung, D. D. L. 2006a. Self-sensing of flexural damage and strain in carbon fiber reinforced cement and effect of embedded steel reinforcing bars. *Carbon* 44(8):1496-1502.

Wen, S. and Chung, D. D. L. 2006b. Spatially resolved self-sensing of strain and damage in carbon fiber cement. *J. Mater. Sci.* 41(15):4823-4831

Wen, S. and Chung, D. D. L. 2006c. Effects of strain and damage on the strain sensing ability of carbon fiber cement", *J. Mater. Civil Eng.* 18(3):355-360.

Wen, S. and Chung, D. D. L. 2007. Piezoresistivity-based strain sensing in carbon fiber reinforced cement. *ACI Mater. J.* 104(2):171-179.